RSC Advances

Silver-nanospheres as a green catalyst for decontamination of hazardous pollutants

Journal:	*RSC Advances*
Manuscript ID	RA-ART-10-2015-021599.R1
Article Type:	Paper
Date Submitted by the Author:	19-Nov-2015
Complete List of Authors:	Vellaichamy, Balakumar; Thiagarajar College, Chemistry Periakaruppan, Prakash; Thiagarajar College, Chemistry
Subject area & keyword:	Nanocatalysis - Catalysis < Catalysis

Journal Name

ARTICLE

Silver-nanospheres as a green catalyst for decontamination of hazardous pollutants

Balakumar Vellaichamy and Prakash Periakaruppan*

Received 00th January 20xx,
Accepted 00th January 20xx

DOI: 10.1039/x0xx00000x

www.rsc.org/

The development of efficient green chemistry route for the synthesis of metal nanoparticles has become a major focus of researchers. The present paper reports a facile, green and one-pot synthesis of silver-nanospheres (Ag-NSs) with high yield and uniform size of 7 nm using *Simarouba glauca* leaf extract (SGLE). The Ag-NSs have been characterized for their morphology, crystallinity and structure using TEM, EDX, XRD, and FT-IR and their formation mechanism discussed. In addition, the decontamination of hazardous pollutants, 4-hydroxynitrobenzene (4-HNB) and 4-nitrophenylamine (4-NPA) with an addition of excess amount of ice cold $NaBH_4$ solution using Ag-NSs as an excellent green catalyst has also been investigated spectrometrically. The reusability of the catalyst is able to be achieved for the reaction even after five cycles.

Introduction

The convenient, cost effective and environmentally friendly green chemistry route for nanomaterials synthesis has generated much interest due to the rapidly-increasing demand for environmental protection. These nanomaterials exhibit their intrinsic electronic properties, high surface-to-volume ratio and can be exploited for a number of applications like sensors, electronics, and especially for catalysis.[1,2] The synthesis of silver nano materials are more important due to their physical properties which can be tailored for a specific application by controlling their size, shape, morphology, orientation, composition and surrounding microenvironments.[3-6] A variety of desired nanostructures with different morphologies including monodispersed nanoparticles,[7-9] nanoprisms,[10] nanocubes,[11] nanowires,[12] nanospheres,[13] nanoleaves[14] and nanodisks[15] have been constructed. Generally, the nanomaterials are prepared by the reduction of silver ions by chemical,[12] electrochemical,[13] radiation,[16] microemulsion,[7] UV irradiation,[17] microwave,[18] photochemical methods,[19] Langmuir–Blodgett,[20] and biological method.[21] However, there is an urgent need to replace the existing methods with clean, non-toxic and environmentally acceptable green chemistry. An environmentally benign solvent and eco-friendly reducing and capping agents are the three vital elements for a complete green synthesis technique. Further, the synthesis of silver nanoparticles using plant extracts is very cost effective, and therefore can be used as an economic and valuable alternative for the large-scale production of metal nanoparticles.

Catalysis is the most important chemical application of metal nanoparticles. Noble metal-catalyzed reduction of nitro groups to amines has been extensively investigated due to its importance in wastewater treatment and organic synthesis.[22-25] The reduction of nitro compounds to amino compounds with an excess amount of $NaBH_4$ has often been used as model reaction to examine the catalytic performance of metal nanoparticles.[26-28] In particular, 4-hydroxynitrobenzene (4-HNB) and 4-nitrophenylamine (4-NPA) have been listed as ''priority pollutants'' by US Environmental Protection Agency (EPA) because of its higher toxicity, solubility and stability in water. 4-HNB and 4-NPA are toxic and bio-refractory compound which can cause several blood disorders, hormonal imbalance, eye irritation and affect central nervous system, liver, kidney and blood of humans and animals.[29, 30] Their disposal in wastewater results in high carcinogenicity, mutagenicity and toxicity to several organisms.[31-35] Hence the decontamination of 4-HNB and 4-NPA acquires a great importance in both environment and industry. The chemical transformation of 4-HNB and 4-NPA via catalytic reduction process is to fabricate the corresponding 4-Hydroxyaminobenzene (4-HAB) and 4-Phenylenediamine (4-PDA), which provides an efficient way to eliminate nitroaromatic pollutants, for that reason the aminoaromatic compounds are very important intermediates in the manufacture of analgesic and antipyretic drugs.

Herein we report a green synthesis of uniform Ag-NSs using *Simarouba glauca* leaf extract (SGLE) without adding any other chemicals. The reaction rates and the surface plasmon resonance (SPR) of formed Ag-NSs were continuously monitored by UV-Visible spectroscopy. The synthesized Ag-NSs was characterized by X-ray diffraction (XRD), FT-IR Spectroscopy (FT-IR), High resolution transition electron microscopy (HR-TEM) and Energy Dispersive X-ray (EDX) spectrometer. The Ag-NSs as an efficient green catalyst has also been investigated for the decontamination of hazardous pollutants, 4-HNB and 4-NPA. The usage of such green synthesized homogeneous Ag-NSs catalyst is energy efficient, cost-effective and eco-friendly which can be an alternate to any chemically synthesized catalyst in the degradation of hazardous pollutants. To date no work has been carried out on the decontamination of 4-HNB and 4-NPA using green synthesized Ag-NSs.

Experimental

Preparation of SGLE

Fresh and healthy SG leaves were collected and rinsed thoroughly first with running tap water followed by deionized water to remove all the dust and other contaminated organic contents and cut into the small pieces. The 100 mg of small pieces of SG leaves was boiled

Department of Chemistry, Thiagarajar College, Madurai-625 009, Tamil Nadu, India.
*Corresponding author. Tel.: +91 9842993931; Fax: +91 4522312375
E-mail address: kmpprakash@gmail.com (P. Prakash)
DOI: 10.1039/x0xx00000x

with 100 mL of deionized water at 90^{0}C for 15 min at room temperature and the extract was thrice filtered using Whatmann filter paper no 1 to remove particulate matter and to get clear solution. The filtered SGLE was pale yellow in color and it was used as reducing as well as stabilizing agent for the synthesis of Ag-NSs. The filtrate solution was stored in the refrigerator at 4^{0}C for further experiments.

Green synthesis of Ag-NSs

5 mL of SGLE was mixed with 10 mL of aqueous solution of 1mM $AgNO_3$ solution at room temperature. The pale yellow colour solution becomes deeper brown within an hour and no noticeable difference in the colour of aqueous silver colloids is observed, which indicates that the bio-reduction process is over within 90 min. The brown colour indicates the formation of Ag-NSs in aqueous solution due to excitation of Surface Plasmon vibration in the metal nanoparticles. The synthesized Ag-NSs were collected by centrifugation at 2000rpm for 15min. and then the filtrate was re-dispersed in water and centrifuged for several times to remove any excess amount of organic contents. Finally the dark brown Ag-NSs were lyophilized in ambient condition. After lyophilisation, the Ag-NSs were stored in screw cap bottle for further characterization.

Catalytic decontamination of hazardous pollutants, 4-HNB and 4-NPA

In a typical experiment, 1.8 mL of 4-HNB (0.1 mM, aqueous solution) was mixed with 0.7 mL of $NaBH_4$ (0.01 M aqueous solution) in a quartz cell (3.0 mL). Then, 0.01mg of Ag-NSs catalyst was added to the mixture of 4-HNB and $NaBH_4$ and the changes in the absorbance of the solution were monitored with a UV-visible spectrophotometer at different time intervals. After the reaction was over, the mixture was centrifuged and washed with deionized water thrice. The resulting catalyst was reused in the next reaction. 4-NPA was also detoxificated by adopting the same procedure.

Characterization

UV-visible spectra were measured using a Jasco (V-560) model UV-visible double beam spectrophotometer.The sample measurements were performed in a 1 cm quartz cuvette at room temperature. The FT-IR spectral measurements were recorded using KBr disc on a JASCO FT-IR 460 Plus spectrophotometer. XRD analysis was carried out by X-ray diffraction unit using Cu Kα radiation (λ = 1.5418o A) on JEOL JDX 8030 X- ray diffractometer.

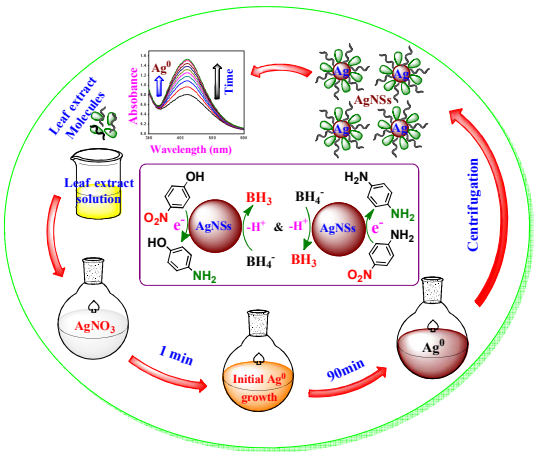

Scheme 1. Synthesis of Ag-NSs using SGLE and its catalytic performance in the decontamination of 4-HNB and 4-NPA.

The size and morphology of the Ag-NSs were examined by transmission electron microscopy (HR-TEM, JEOL JEM 2100) model instruments. Energy Dispersive X-ray (EDX) spectrometer attached to the transmission electron microscope was used for elemental analysis. All experiments were carried out at room temperature.

Results and discussion

Characterization

Since green synthesized Ag-NSs exhibit strong absorption band due to SPR in the visible region at about 400 to 480 nm, the electronic spectroscopy is one of the simplest techniques to characterize them. The formation of Ag-NSs was visually identified by means of change in color of reaction mixture from pale yellow to yellowish brown to dark brown, depending on the intensity and hence the number of nanospheres (shown in Fig.1a). UV–visible absorbance spectral values at 420 nm confirm the bioreduction of silver ions to metallic silver (Fig.1b (curve a-j)) by using SGLE. The SPR peak appears immediately after the addition of the plant extract. The formation of Ag-NSs with different time intervals of 1, 10, 20, 30, 40, 50, 60, 70, 80 and 90 min indicate that there is no shift in the absorption peak position. Only SPR intensity increases, which indicates the continuous reduction of the silver ions and the increase in absorbance signifies the formation of uniform Ag-NSs. In the synthesis of metal nanoparticles using plant extract, the reaction time is a major drawback for several biosynthetic procedures.[36] But here the absorption peak steadily increases and after 90 min there is no increase, which confirms that the reaction is completed within 90 min. The kinetics of this reduction was followed by monitoring the absorbance intensity of SPR peak as a function of time and the intensity of color which does not intensify after 90 min which is established by Fig. 1c. The absorption recorded after 24h shows the same intensity, which is shown in Fig. 1d. The observed SPR band at 420 nm is a strong evidence for the successful formation of Ag-NSs. Scheme 1 shows the detailed mechanis m of green synthesized uniform Ag-NSs and its catalytic performance in the reduction of 4-HNB and 4-NPA.

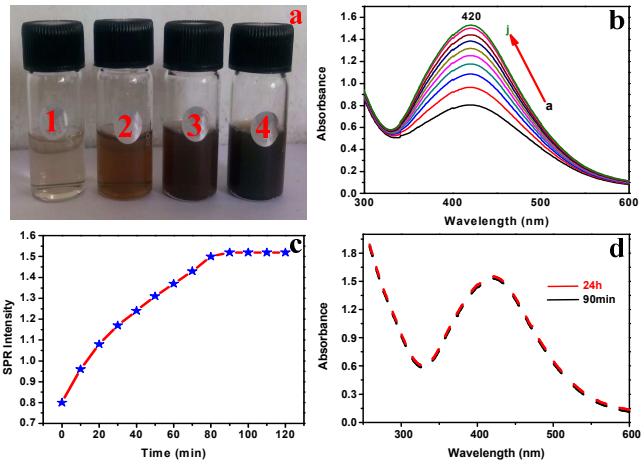

Fig. 1 (a) shows the photographs of Ag-NSs at different time intervals (1) leaf extract only, (2) having added $AgNO_3$ after 10 min, (3) 50 min and (4) 90 min; (b) UV –Visible spectra of Ag-NSs as a function of time with time interval of 10 min. (curve a to j); (c) Plot of the intensity of the SPR at 420 nm against the reaction time; (d) UV –Visible spectra of Ag-NSs after 90min (black line) and after 24h (red line).

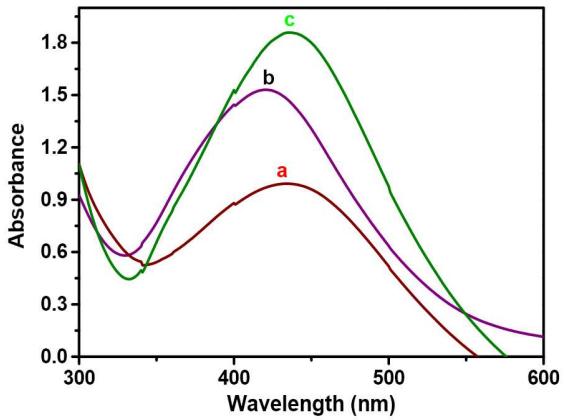

Fig. 2 UV-Visible spectra with different concentrations of $AgNO_3$ (a) 0.05, (b) 1.0 and (c) 1.5 mM.

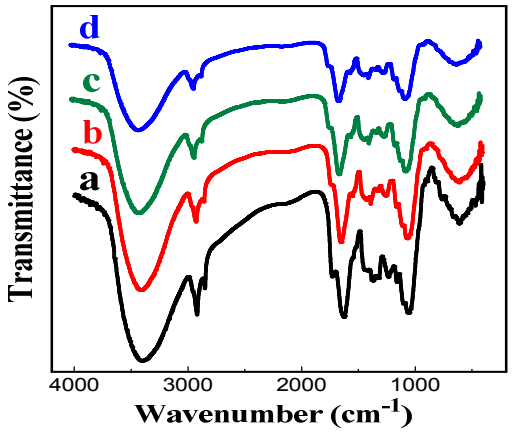

Fig. 3 FT-IR spectra of SGL (a), having added $AgNO_3$ to SGLE after 10 min (b), 50 min (c) and 90 min (d).

The nano-spheres with 7 nm size was obtained with 1 mM concentration of $AgNO_3$. In order to decide if the concentration of $AgNO_3$ influences the particle size, experiments were carried out by changing the concentration of $AgNO_3$ keeping the leaf extract concentration constant. The absorption shifts to longer wave length when the concentration of $AgNO_3$ is either increased or decreased. Red shift usually causes anisotropy. Hence, in this study, the concentration of $AgNO_3$ (1 mM) is the driving force that controls the particle size, which is supported by other studies [37-40].

The FT-IR measurements were carried out to find out the possible molecules present in the leaf extract of SG which are responsible for the reduction of silver ions and stabilization of the synthesized Ag-NSs. There are several characteristic peaks which appear in Fig. 3a. 1622 cm^{-1} is the C=O stretching vibration of carbonyl and carboxylic group of amide I in SG leaf proteins.[39] The intense peak at 3409 cm^{-1} is due to the ⁻OH stretching vibration of hydroxyl functional groups of polyphenols and alcohols and ⁻NH stretching vibrations of amide (II) (or) amine. The peaks at 2925 and 2850 cm^{-1} are characteristic of stretching vibrations of methyl groups or C=H stretching vibrations of aldehydic amine groups and C–O stretching vibrations of esters appear at 1731 cm^{-1}. The peaks observed at 1427 and 1058 cm^{-1} are the bending vibration of C–O–H groups and the anti-symmetric stretching band of C–O–C groups of polysaccharides and/or chlorophyll and the peaks around 1236 cm^{-1} are the bending vibration of C–N groups, amide II and III bands in the proteins. The C–O stretching vibration of polyols around at 1232 cm^{-1} and the peak appearing at 1152 cm^{-1} could be attributed to a carbonyl group as in aldehydic and ketonic group.[40] The peak at 660 cm^{-1} is the plane bending vibration of N–H groups in the proteins. The strength and intensity of the all peaks are obviously weakened. After reduction with silver ions (Fig. 3b, c and d) the strength of the peak at 3409 cm^{-1} represents the presence of proteins/enzymes or polysaccharide components and assigned to the vibration of –N–N– groups, the stretching vibrations of methyl groups or C=H stretching vibrations of aldehydic amine groups are observed at 2925 and 2850 cm^{-1} and the peak at 660 cm^{-1} indicates the reduction of the silver ions coupled to the oxidation of the amine components. Meanwhile the intensity of the above mentioned hydrogen bonded N–H groups weakens obviously. The observed results indicate the possible involvement of above mentioned groups in the Ag-NSs.[23] The peak at 1622 cm^{-1} is due to C=O stretching vibration of carbonyl and carboxylic groups present in amide-I linkage of proteins.

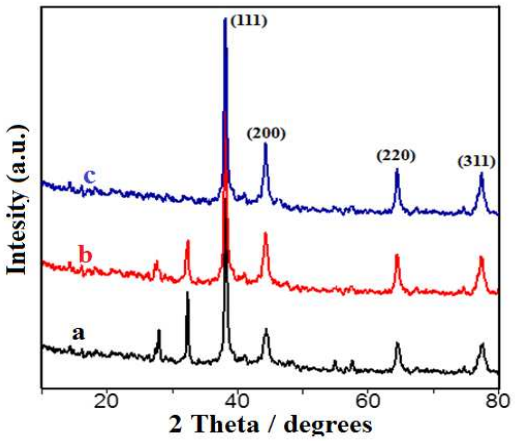

Fig. 4 XRD Patterns of Ag-NSs synthesized at different time intervals (a) 10 min, (b) 50 min and (c) 90 min.

As indicated by the FT-IR data, the plant extract contains phyto chemicals and the functional groups like alcohol or phenol, amine, amide (I) and (II), aldehydes, polyol and methylene groups. The close observation of shift and reduction in intensity of the peaks from 1622 to 1640 cm^{-1} suggests that the amide-I linkage of protein groups may be present on the surface of the Ag-NSs[39,40].

The crystalline nature and orientation of green synthesized Ag-NSs was confirmed by XRD analysis (Fig.4 a-c). The XRD pattern of time correlated Ag-NSs indicates four different sharp diffraction peaks at 2θ values: 38.1^0, 44.2^0, 64.2^0 and 77.4^0, which correspond to lattice planes of (1 1 1), (2 0 0), (2 2 0) and (3 1 1) with face centered cubic (fcc) structure of metallic silver, which is in good agreement with reference to the unit cell of the fcc structure and is consistent with Joint Committee on Powder Diffraction Standards (JCPDS) data [No. 04-0783]. Fig. 4 (a-c) shows the XRD pattern of Ag-NSs with different time intervals of 10, 50 and 90 min. In curves 'a' and 'b', some unassigned peaks appear at 28.3^0 and 32.2^0 which are due to the crystallization of bioorganic phases which occur on the surface of the nanospheres[41-43]. In Fig. 4 (curve c), sharp and strong signals of patterns appear which evidences that the products are nanosized and well crystallized.

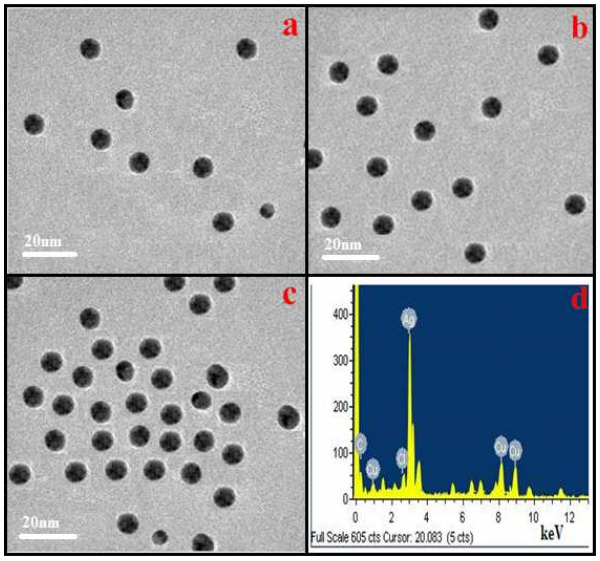

Fig. 5 HR-TEM images of Ag-NSs synthesized at different time intervals (a) 10 min, (b) 50 min and (c) 90 min and EDX spectrum of Ag-NSs.

As time increases, the formations of Ag-NSs planes increases and the unassigned peaks decrease and finally disappear. Among the lattice planes, the peak corresponding to (1 1 1) plane is more intense than other planes suggesting it as a predominant orientation. The green synthesized Ag-NSs is essentially pure and the values of average crystalline size has been estimated by using Debye-Scherrer equation,[44]

$$D = \frac{K\lambda}{\beta}\cos\theta$$

where K denotes the Scherrer's constant (K = 0.94), λ is the X-ray wavelength, β is the full-width at half-maximum (FWHM) of diffraction line in radian and θ is half diffraction angle. The width of the (111) peak was employed to calculate the average crystalline size of the Ag-NSs using the above Scherrer formula. The calculated average size of the Ag-NSs is 7 nm, which precisely matches with the particle size obtained from HR-TEM image (Fig. 5 (a-c)).

The surface morphology, size and shape of the Ag-NSs were identified by HR-TEM images and they are shown in Fig. 5. Fig. 5 (a-c) clearly shows that TEM images of Ag-NSs with different time intervals of 10, 50 and 90 min.

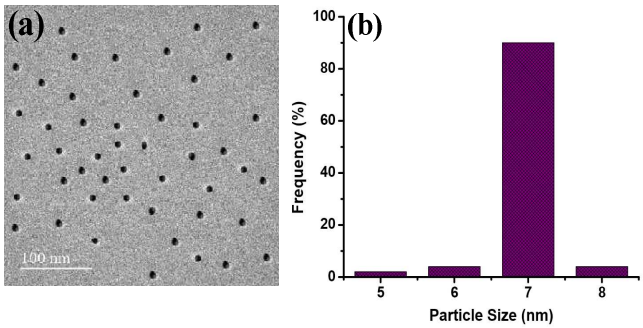

Fig. 6 (a) HR-TEM image with lower magnification of Ag-NSs and (b) Histogram showing particle size distribution.

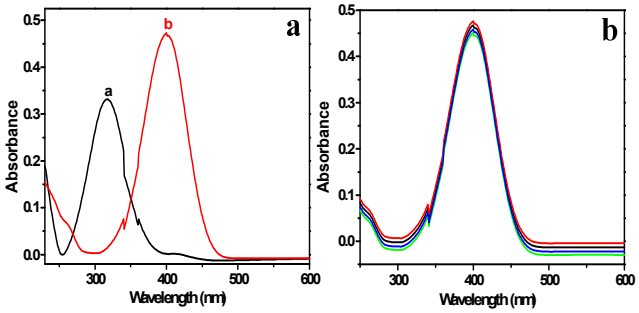

Fig. 7 (a) UV–vis spectrum of 4-HNB (curve a) and 4-HNB with $NaBH_4$ (curve b); (b) 4-HNB with $NaBH_4$ without addition of any catalyst.

The micrographs clearly indicate that the Ag-NSs possess uniform unagglomerated nanospheres with the size of 7 nm. As the time increases, the formation of Ag-NSs also increases. The 420 nm band corresponds to the Ag-NSs and there is no shift in the SPR band which qualitatively indicates the formations of Ag-NSs.[36] Fig. 5d shows the chemical analysis of the synthesized Ag-NSs by means of EDX which confirms the existence of Ag. Furthermore Fig. 6 (a) shows the HR-TEM image with lower magnification of Ag-NSs and (b) size distribution histogram. The TEM results are well supported by all other experimental results of formation of green synthesized Ag-NSs.

Catalytic decontamination

To test the efficiency of Ag-NSs, its catalytic reduction was monitored as follows. The catalytic reduction of 4-HNB and 4-NPA with an addition of excess amount of freshly prepared ice cold $NaBH_4$ was done to evaluate the catalytic performance of metal nanoparticles.

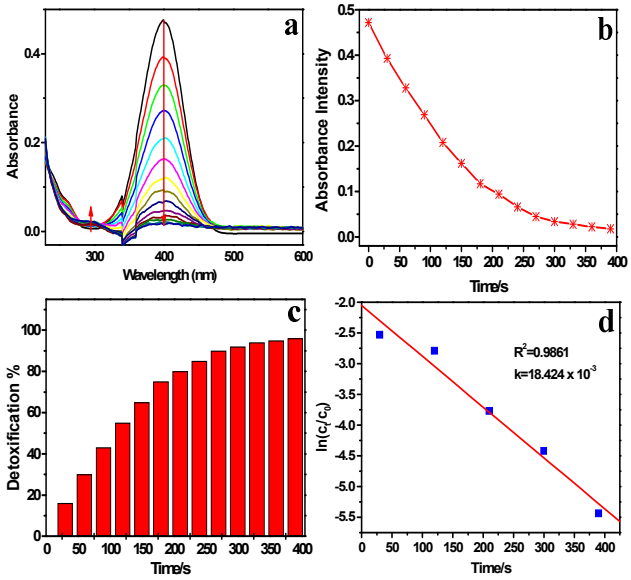

Fig. 8 (a) UV–vis spectra of 4-HNB reduction in the presence of $NaBH_4$ and Ag-NSs; (b) Plot of absorbance intensity Vs time; (c) Plot of the reduction % Vs time; (d) The plot of $\ln(C_t/C_0)$ against the reaction time for reduction kinetics of 4-HNB in the presence of Ag-NSs.

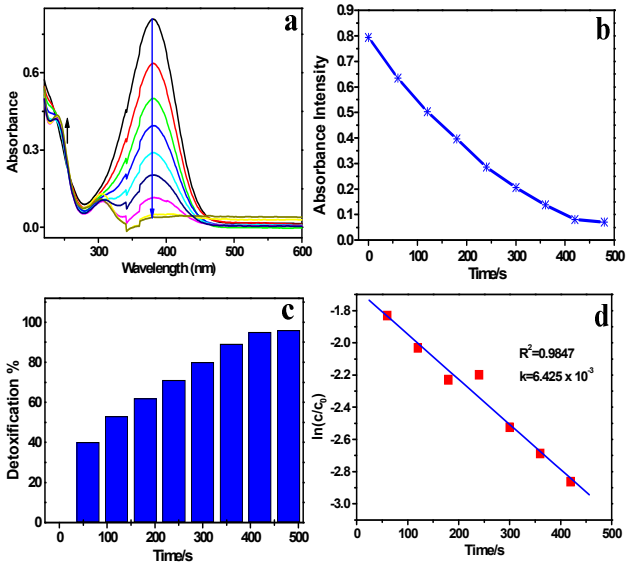

Fig. 9 (a) UV–vis spectra of 4-NPA reduction in the presence of $NaBH_4$ and Ag-NSs; (b) Plot of absorbance intensity Vs time; (c) Plot of the reduction % Vs time; (d) The plot of $\ln(C_t/C_0)$ against the reaction time for reduction kinetics of 4-NPA in the presence of Ag-NSs.

Metal nanoparticles can successfully catalyze the decontamination of nitro compounds by acting as an electronic relay system wherein the electron-transfer from the donor BH_4^- to acceptor nitro groups. As shown in Fig. 7a and 9a, aqueous solution of 4-HNB shows absorption peak at 317 nm and 4-NPA at 380 nm due to the n-π* transition. It is observed that the absorption peak of 4-HNB is red-shifted from 317 to 400 nm (Fig. 7a) immediately upon the addition of $NaBH_4$ solution which corresponds to a color change from pale yellow to yellow, due to the formation of the 4-nitrophenolate ion under alkaline mediums.[26, 27] Though no shifting of peak in 4-NPA at 380 nm is observed, the intensity of peak decreases after the addition of $NaBH_4$. In the absence of green catalyst the 4-HNB adsorption peak at 400nm remains unaltered with time, indicating that the reduction reaction does not proceed and the color of the solution stays yellow only (Fig. 7b). In the absence of green catalyst the thermodynamically favourable reduction of the nitro compounds was not observed under the experimental

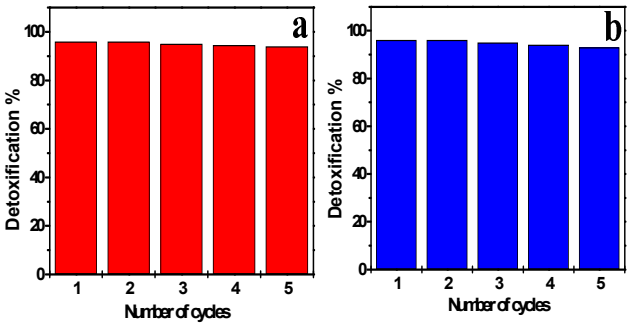

Fig. 10 (a) Plot of 4-HNB reduction % Vs number of cycles; (b) Plot of the 4-NPA reduction % Vs number of cycles.

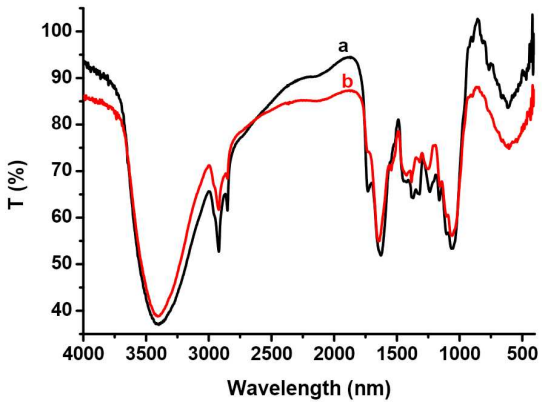

Fig. 11 FTIR spectra of Ag-NSs of pre (a) and post (b) catalysis.

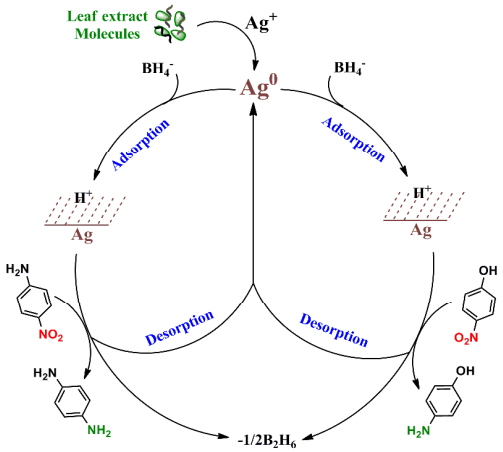

Scheme 2. The reaction mechanism for the decontamination of 4-HNB and 4-NPA catalyzed by Ag-NSs in the presence of $NaBH_4$.

condition. Moreover suitable amount of catalyst (0.01mg) when added into the solution, the reduction reaction is initiated by the decolorization of the 4-nitrophenolate and 4-NPA solution. Further the absorption peak intensity at 400 and 380nm gradually decreases with a new adsorption peak appearing at 295 nm corresponding to the formation 4-HAB, and 240 and 305 nm corresponding to 4-phenylenediamine (4-PDA).[45,46] From Fig. 8a and 9a, it can be seen that the absorption peaks at 400 and 380nm indicate the gradual conversion of 4-nitrophenolate and 4-NPA to 4-HAB and 4-PDA without any by-products formation.[47, 48] The complete conversion of 4-nitrophenolate to 4-HAB and 4-NPA to 4-PDA can be established by the perfect color change of the solution from yellow to colorless. The reaction kinetics was monitored easily from the time-dependent absorption spectra as shown in Fig. 8a and 9a. Fig. 8 (b-c) and 9 (b-c) illustrate the absorbance intensity and decontamination percentage vs. time plots towards 4-HNB to 4-HAB and 4-NPA to 4-PDA reduction using Ag-NSs as a green catalyst. The reaction kinetics can be described as $-\ln(C_t/C_0) = kt$, where k is the rate constant at a given temperature and t is the reaction time. C_0 and C_t are the 4-HNB concentration at the beginning and at time t, respectively.

Journal Name

ARTICLE

Table 1 Catalytic performance of different silver catalysts for the reduction of 4-HNB and 4-NPA

Substrate	Silver catalysts	Size (nm)	[Catalyst] (mg)	K (S^{-1})	κ (S^{-1} g^{-1})	Conversion time (Sec)	References
4-HNB	Ag	50-200	$18.5x10^{-3}$	9.68×10^{-3}	523.24	300	49
	TAC-Ag	90	4.0	5.19×10^{-3}	1.30	430	50
	TSC-Ag	50-100	4.0	3.64×10^{-4}	0.09	2860	50
	Ag-NP/C	10-300	1.0	$1.69x\ 10^{-3}$	192.05	1500	51
	Fe_3O_4-@SiO_2-Ag	200	1.0	7.67×10^{-3}	7.67	480	52
	Fe_3O_4/SiO_2-Ag	40-283	0.02	5.50×10^{-3}	275	-	53
	AgNP-PG-5K	18	0.004	5.50×10^{-3}	1375	640	54
	Fe_3O_4-@C@Ag-Au	120	0.01	15.80×10^{-3}	1580	750	55
	Fe_3O_4-@C@Ag	100	0.01	3.72×10^{-3}	372	1080	55
	Sponge-like Ag	50-150	0.01	$13.1x10^{-3}$	1310	240	56
	Ag-NSs	7	0.01	$18.\ 42x10^{-3}$	1842	360	**Present work**
4-NPA	Fe_3O_4@Nico@Ag	20-50	-	-	30.6	420	57
	Ag Spheres	10-48	850	$25.2x\ 10^{-3}$	-	480	28
	Ag	84	-	-	-	1620	43
	Fe_3O_4/SiO_2/Ag	40	-	-	-	-	58
	Ag-NSs	7	0.01	6.425×10^{-3}	642	480	**Present work**

As expected, a good linear correlation of $\ln(C_t/C_0)$ vs. reaction time t, up to 96% was obtained (Fig. 8c). The kinetic rate constant k is calculated from the slopes of the linear sections of the plots and is given in Fig. 8d and 9d. The value of k is calculated to be for 4-HNB: 18.424×10^{-3} S^{-1} and for 4-NPA: 6.425×10^{-3} S^{-1} at room temperature. The catalytic studies were performed using Ag-NSs, which exhibit higher catalytic performance compared to other earlier reported results, which are summarized in Table 1.[49-57,28,43,58] It is mentioned here that the well mono dispersed metal nanoparticles solution is relatively smaller in size (7 nm). The smaller size consists of intrinsic electronic properties, high surface to volume ratio and more exposed Ag atoms on the surface, and these exposed atoms strongly act as the catalyst. Recyclability and stability are important characteristics of a good catalyst. In order to investigate the recyclability of the Ag-NSs, the same catalyst was utilized repeatedly for five times for the reduction reaction. After each use, the catalyst was centrifuged, washed and dried for the next cycle of catalysis. The catalyst exhibits high activity for the conversion even after five cycles as shown in Fig. 10. Such results indicate that the presence of SGLE is sufficient to stabilize the catalytic performance of silver nanoparticles by preventing their aggregation and therefore the Ag-NSs can act as a good catalyst. FT-IR spectra of Ag-NSs of pre and post catalysis reaction are given in Fig. 11, which indicates that the functional groups on the surface of the nanoparticles play no role in promoting catalysis. The nanoparticles successfully catalyse the reaction by acting as an electronic relay system wherein the electron-transfer takes place from the donor BH_4^- to acceptor nitro groups.[26,27, 49-58]. The mechanism of decontamination of 4-HNB and 4-NPA to 4-HAB and 4-PDA by $NaBH_4$ in the presence of Ag-NSs are demonstrated in scheme 2.

Conclusions

In summary, a simple green synthesis and characterization of Ag-NSs for the decontamination of 4-HNB and 4-NPA have been demonstrated. The formed Ag-NSs is uniform in size of 7nm. The value of rate constant, k for reduction is calculated to be, for 4-HNB: 18.424×10^{-3} S^{-1} and for 4-NPA: 6.425×10^{-3} S^{-1} at room temperature. The catalyst exhibits high activity for the conversion even after five cycles. The synthesized Ag-NSs as green catalyst with high reusability is very efficient, stable and cost-effective for the decontamination of hazardous pollutants.

References

1 G. Cepria, W. R. Córdova, J. J. Lamana, F. Laborda and J. R. Castillo, *Anal. Meth.,* 2014, 6, 3072-3078.
2 F. Frederix, J-M. Friedt, K-H. Choi, W. Laureyn, A. Campitelli, D. Mondelaers, G. Maes, and G. Borghs, *Anal. Chem.,* 2003, 75, 6894-6900.
3 A. Abbas, M. J. Linman and Q. Cheng, *Biosens. Bioelectron.,* 2011, 26, 1815-1824.
4 P. Alexandridis, *Chem. Eng. Technol.,* 2011, 34, 15-28.
5 C. M. Cobley, J. Chen, E. C. Cho, L. V. Wang and Y. Xia, *Chem. Soc. Rev.,* 2011, 40, 44-56.
6 T. K. Sau and A. L. Rogach, *Adv. Mater.,* 2010, 22, 1781-1804.
7 D. Zhang, X. Liu, X. Wang, X. Yang and L. Lu, *Phys. B Condens. Matter.,* 2011, 406, 1389-1394.

8 R. Ramanathan, A. P. O'Mullane, R. Y. Parikh, P. M. Smooker, S. K. Bhargava and V. Bansal, *Langmuir,* 2011, 27, 714–719.
9 V. Bansal, A. Bharde, R. Ramanathan and S. K. Bhargava, *Adv. Colloid Interface Sci.,* 2012, 179–182, 150–168.
10 X. Dong, X. Ji, J. Jing, M. Li, J. Li and W. Yang, *J. Phys. Chem. C,* 2010, 114 2070-2074.
11 D. Yu and V. W-W. Yam, *J. Am. Chem. Soc.,* 2004, 126, 13200-13201.
12 Y. Sun, Y. Yin, B. T. Mayers, T. Herricks and Y. Xia, *Chem. Mater.,* 2002, 14, 4736-4745.
13 B. Yin, H. Ma, S. Wang and S. Chen, *J. Phys. Chem. B,* 2003, 107, 8898-8904.
14 L. Li and Q. Wang, *ACS Nano,* 2013, 7, 3053-3060.
15 M-R. Raquel, N. O. Nunez, E. D. Barriga-Castro and C. Luna, *RSC Adv.,* 2013, 3, 20765-20771.
16 N. M. Dimitrijevic, D. M. Bartels, C. D. Jonah, K. Takahashi and T. Rajh, *J. Phys. Chem. B,* 2001, 105, 954-959.
17 D. Spadaro, E. Barletta, F. Barreca, G. Curro and F. Neri, *Appl. Surf. Sci.,* 2010, 256, 3812-3816.
18 M. N. Nadagouda, T. F. Speth and R. S. Varma, *Acc. Chem. Res.,* 2011, 44, 469-478.
19 A. Callegari, D. Tonti and M. Chergui, *Nano Lett.,* 2003, 3, 1565-1568.
20 L. Zhang, Y. H. Shen, A. J. Xie, S. K. Li, B. K. Jin and Q. F. Zhang, *J. Phys. Chem. B,* 2006, 110, 6615-6620.
21 R. R. Naik, S. J. Stringer, G. Agarwal, S. Jones and M. O. Stone, *Nat. Mater.,* 2002, 1, 169-172.
22 F. Coccia, L. Tonucci, D. Bosco, M. Bressan and N. d'Alessandro, *Green Chem.,* 2012, 14, 1073-1078.
23 F. Dong, W. Guo, S-K. Park and C-S. Ha, *Chem. Commun.,* 2012, 48, 1108-1110.
24 P. Zhang, Y. Sui, G. Xiao, Y. Wang, C. Wang, B. Liu, G. Zou and B. Zou, *J. Mater. Chem. A,* 2013, 1, 1632-1638.
25 J. Wang, X-B. Zhang, Z-L. Wang, L-M. Wang, W. Xing and X. Liu, *Nanoscale,* 2012, 4, 1549-1552.
26 Y. Yang, Y. Ren, C. Sun and S. Hao, *Green Chem.,* 2014, 16, 2273-2280.
27 J. Li, C-Y. Liu and Y. Liu, *J. Mater. Chem.,* 2012, 22, 8426-8430.
28 R. Vadakkekara, M. Chakraborty and P. A. Parikh, *Colloids Surf. A,* 2012, 399, 11-17.
29 E. Pocurull, R.M. Marce and F. Borrull, *J. Chromatogr. A,* 1996, 738, 1–9.
30 W.B. Zhang, X.M. Xiao, T.C. An, Z.G. Song, J.M. Fu, G.Y. Sheng and M.C. Cui, *J. Chem. Technol. Biotechnol.,* 2003, 78, 788-794.
31 S. Zok, G. Goerge, W. Kalsch and R. Nagel, *Sci. Total. Environ.,* 1991, 109-110, 411-421.
32 R.S. Nair, C.S. Auletta, R.E. Schroeder and F.R. Johannsen, *Fundam. Appl. Toxicol.,* 1990, 15, 607-621.
33 G. Wang, X. Zhang, C. Yao and M.Tian, *Drug Chem. Toxicol.,* 2010, 33, 238-243.
34 K.L. Wu, X.W. Wei, X.M. Zhou, D.H. Wu, X.M. Liu, Y. Ye and Q. Wang *J. Phys. Chem. C,* 2011, 115, 16268-16274.
35 R.Z. Chen, Q.Q. Wang, Y. Du, W.L. Xing and N.P. Xu, *Chem. Eng. J,* 2009, 145, 371-376.
36 A. Gangula, R. Podila, M. Ramakrishna, K. Lohith, J. Chelli and M. R. Apparao, *Langmuir,* 2011, 27, 15268-15274.
37 S. Sana, V. Badineni, S. Arla and V. NaiduBoya, *Mater. Lett.,* 2015, 145, 347–350.
38 M. Zargar, K. Shameli, G. R. Najafi and F. Farahani, *J. Ind. Eng. Chem.,* 2014, DOI: http://dx.doi.org/10.1016/j.jiec.2014.01.016.
39 J. Kasturi, S. Veerapandian and N. Rajendran, *Colloids. Surf. B,* 2009, 68, 55–60.
40 R. Emmanuel, K. Chelladurai, S-M. Chen, P. Selvakumar, S. Padmavathy, and P. Prakash, *J. Hazard. Mater.,* 2014, 279, 117-124.
41 G. Singhal, R. Bhavesh, K. Kasariya, A. R. Sharma and R. P. Singh, *J. Nanopart. Res.,* 2011, 13, 2981-2988.
42 J. P. Ruparelia, A. Chatterjee, S. P. Duttagupta and S. Mukherji, *Acta. Biomater.,* 2008, 4, 707-716.
43 P. Velmurugan, S. Sivakumar, S. Young-Chae, J. Seong-Ho, Y. Pyoung-In, S. Jeong-Min, and H. Sung-Chul, *J. Ind. Eng. Chem.,* 2015, DOI: http://dx.doi.org/10.1016/j.jiec.2015.06.031.
44 B. D. Cullity, *Elements of X-ray Diffraction,* 2nd ed., Addition-Wesley, Menlo Park, CA, 1978.
45 X. Huang, X. P. Liao and B. Shi, *Green. Chem.,* 2011, 13, 2801-2805.
46 Q. Zhou, G. Qian, Y. Li, G. Zhao, Y. Chao and J. Zheng, *Thin Solid Films,* 2008, 516, 953-956.
47 Y. H. Deng, Y. Cai, Z. K. Sun, J. Liu, C. Liu, J. Wei, W. Li, C. Liu, Y. Wang and D. Y. Zhao, *J. Am. Chem. Soc.,* 2010, 132, 8466-8473.
48 S. Jana, S. K. Ghosh, S. Nath, S. Pande, S. Praharaj, S. Panigrahi, S. Basu, T. Endo and T. Pal, *Appl. Catal. A,* 2006, 313, 41-48.
49 S. Gu, W. Wang, F. Tan, J. Gu, X. Qiao and J. Chen, *Mater. Res. Bull.,* 2014, 49,138-143.
50 M. H. Rashid and T. K. Mandal, *J. Phys. Chem. C,* 2007, 111, 16750-16760.
51 S. Tang, S. Vongehr and X. Meng, *J. Phys. Chem. C,* 2009, 114, 977.
52 Y. Chi, Q. Yuan, Y. Li, J. Tu, L. Zhao, N. Li and X. Li, *J. Colloid Interface Sci.,* 2012, 383, 96-102.
53 K. S. Shin, Y. K. Cho, J-Y. Choi and K. Kim, *Appl. Catal. A,* 2012, 413–414, 170-175.
54 B. Baruah, G. J. Gabriel, M. J. Akbashev and M. E. Booher, *Langmuir,* 2013, 29, 4225-4234.
55 Q. An, M. Yu, Y. Zhang, W. Ma, J. Guo and C. Wang, *J. Phys. Chem. C,* 2012, 116, 22432-22440.
56 Y. Mao, J. Wei, C. Wang, Y. Feng, H. Yang, and X. Meng, *Mater. Lett.,* 2015, 154, 47-50.
57 U. Kurtan, Md. Amir and A. Baykal, *Chin. J. Catal.,* 2015, 36, 705–711.
58 M. Abbas, S.R. Torati, C. Kim, *Nanoscale*, 2015, DOI: 10.1039/C5NR02680F.

Graphical Abstract